Int. J. Electrochem. Sci., 14 **(2019)** 7088 – 7103, doi: 10.20964/2019.08.60

International Journal of
ELECTROCHEMICAL
SCIENCE
www.electrochemsci.org

A Sandwich-Structure Composite Membrane as Separator with High Wettability and Thermal Properties for Advanced Lithium-Ion Batteries

Yang Li[1,2], *Jiang Cao*[2,3,*], *Qi Liu*[2], *Aoxuan Wang*[1,*], *Baohua Li*[2]

[1] State Key Laboratory of Chemical Engineering, School of Chemical Engineering and Technology, Tianjin University, Tianjin, 300350, China
[2] Division of Energy and Environment, Engineering Laboratory for the Next Generation Power and Energy Storage Batteries, Graduate School at Shenzhen, Tsinghua University, Shenzhen 518055, China
[3] R&D Center, Shenzhen Senior Technology Material Co., LTD, Shenzhen 518106, China
[*]E-mail: aoxuanwang@tju.edu.cn , kos3123@163.com

Received: 2 April 2019 / *Accepted:* 31 May 2019 / *Published:* 30 June 2019

Lithium-ion batteries with high energy density and environmental friendliness have attracted considerable interest for reseachers in recent years. However, the conventional polyolefin separators with poor electrolyte wettability and low thermal stability limited the further development of lithium-ion batteries. Here we designed a porous poly(m-phenylene isophthalamide) (PMIA) layer, embedded with high-dispersed TiO_2-P(MMA-AA-BA) (TP) nanohybrid, on both sides of a polyethylene (PE) membrane by a facile nonsolvent-induced phase inversion process to improve the electrolyte wettability and thermal stability of the PE separator. The TP nanoparticles can disperse uniformly in PMIA layer. Due to the inherent high-heat resistance and good affinity to the liquid electrolyte of PMIA and nanohybrid, this (TP-PMIA)-modified PE (TP-PMIA@PE) membrane exhibits high porosity, high ionic conductivity, improved thermal resistance and superior interfacial stability, which can endow the composite membrane-based Li/$LiFePO_4$ cell with good capacity retention and superior rate capability. The as-prepared composite membrane can serve as a promising separator for high-safety and high-performance lithium-ion batteries.

Keywords: Poly (m-phenylene isophthalamide); Nanohybrid ; Phase inversion process; Separator; Lithium-ion batteries

1. INTRODUCTION

In the past decades, lithium-ion batteries (LIBs) have been widely applied in portable electronic, electric vehicles and energy storage systems due to their high energy density, excellent cycle life, low self-discharge rate and environmental friendliness [1,2]. A traditional lithium-ion battery is mainly

composed of cathode, anode, separator and electrolyte [3,4]. The separator is a key component in a lithium-ion battery, which is used to prevent short circuit by separating the cathode and anode and allow lithium-ions transport between the electrodes during the charging and discharging processes. Therefore, the property of separator is vital for the battery performance [5,6].

Up to now, the commercial microporous polyolefin separators, such as polypropylene (PP), polyethylene (PE) and their composite membrane (PP/PE/PP), have been widely used in LIBs, due to their good chemical stability, excellent mechanical strength as well as the acceptable cost. However, some inherent drawbacks of polyolefin separators, including low porosity, inferior thermal stability and poor electrolyte wettability, may hinder their application for advanced LIBs to some extent [7]. The low porosity and poor electrolyte wettability of polyolefin membranes are derived from their intrinsic nonpolar properties, which may lead to low ionic conductivity, high cell resistance and poor rate performance of the LIBs. In particular, the low melting point of polyolefin separators makes them suffer great thermal shrinkages when the batteries work under high temperatures, leading to internal short circuit and even ignition or explosion [8]. To solve the abovementioned shortcomings of polyolefin separators, extensive efforts have been devoted to surface modification of polyolefin separators. One effective method is to introduce inorganic nanoparticles coating layers onto the membrane surfaces, such as silicon dioxide (SiO_2) [9,10], aluminum oxide (Al_2O_3) [11], zirconia (ZrO_2) [14] and titanium dioxide (TiO_2) [12,13] etc. The nano-sized inorganic particles can significantly enhance the thermal stability and electrolyte wettability of separators. For example, Kim et al. introduced an amino-functionalized SiO_2 particles to the surface of PE separator. The obtained composite membrane exhibited good electrolyte wettability, high ionic conductivity and enhanced thermal stability, which showed superior cycling stability and thermal safety of LIBs [9]. Zhao et al. developed a ceramic coating separator by introducing Al_2O_3 powder and thermal stable polymer binder (polyimide) onto the surface of a PE membrane, leading to the improved safety and high capacity retention for LIBs [11]. Although the composite membranes with ceramic coating possess excellent electrolyte wettability and good thermal stability, a certain amount of ceramic nanoparticles will aggregate and inevitably block the pores of the polymer matrix. Moreover, the applied binders are easily swelling and gelling in the liquid electrolyte, resulting in shedding of particles from the substrate. The polymer-based coating is another strategy to modify the polyolefin membranes, including aramid nanofiber (ANF) [15], polybenzimidazole (PBI) [16], polydopamine (PDA) [17]. By introducing the polymer onto the surface of polyolefin membranes, the prepared composite membranes exhibit high thermal stability and good affinity with liquid electrolyte. Nevertheless, this method may also lead to some drawbacks, such as pore blocking and multistep operations.

It is well known that the aramid possesses high strength, high flame resistance, superior heat resistance and high electrical insulation, which is widely used as electrical insulating materials, special protective apparels, high temperature filter materials, etc [18-20]. Poly (meta-phenylene isophthalamide) (PMIA), also widely known as meta-aramid, exhibits high mechanical property and superior thermal stability (up to 400 °C). In addition, the PMIA polymer may have superior wettability with liquid electrolyte due to the polar carbonyl groups in it [21]. In recent years, some researchers have used PMIA or PMIA-based composite membranes as separators of LIBs, such as the PVdF/PMIA/PVdF nanofibrous composite membrane [22], F-doped PMIA nanofibrous membrane [23], the SiO_2/PMIA nanofiber

membrane [24]. All of these preparation methods are sophisticated, time-consuming and high manufacturing cost, which are not desirable for the large-scale application. Zhu et al. prepared a microporous PMIA separator by phase separation process [25]. Although the PMIA separator showed high thermal stability, which was beneficial for the safety of batteries, it exhibited no thermal shutdown function and the cost was relatively high.

In this paper, we designed a composite membrane with the three-dimensional (3D) porous TP-PMIA layers on both sides of a PE membrane by a facile phase inversion method with low cost, combining the advantages of polymer and inorganic nanoparticles. A small amount of TiO_2 nanoparticles are distributed uniformly and 3D porous structure can avoid pore blocking of PE matrix effectively. Compared with the bare separator, the obtained porous composite membrane exhibits excellent electrolyte wettability and higher dimensional thermal stability. Thus, the cells assembled with the composite membranes perform high interfacial stability, stable cycle performance and superior rate capability. In addition, the composite membrane shows a shutdown function at high temperature due to the low-melting PE layer. The characterization of the composite membrane was investigated in this paper.

2. EXPERIMENTAL

2.1. Materials

Poly(m-phenylene isophthalamide) (PMIA) was obtained from Teijin Ltd., Japan. N, N-Dimethylacetamide (DMAc) and Lithium chloride (LiCl) was supplied by Aladdin Industrial Co., China. Methyl methacrylate (MMA), acrylic acid (AA) and butyl methacrylate (BA) were provided from Sinopharm Chemical Reagent Co.,Ltd., China. The potassium persulfate and tritonX-100 were purchased from Shanghai Aladdin Biochemical Technology Co., Ltd., China. TiO_2 nanoparticals were purchased from Hangzhou Wanjing New Materials Co., Ltd., China. The microporous polyethylene (PE, thickness 12 μm) membrane were purchased from Shenzhen Xingyuan Materials Technology Co., Ltd., China., which were used as commercial separators of lithium-ion batteries for a contrasting test. All the chemical reagents were used directly without further purification.

2.2. Synthesis of TP nanospheres

In this experiment, a certain amount of TiO_2 nanopaticals were dispersed in deionized water by ultrasonication. The mixture of methyl methacrylate, acrylic acid and butyl methacrylate (MMA-AA-BA) was added to the aqueous solution with mechanical stirring (MMA-AA-BA: TiO_2=80: 20, in mass). Then, the emulsifying agent (tritonX-100) and the initiator (potassium persulfate) were also added slowly to the solution. The emulsion polymerization was carried out in oven for 4 h at 85 °C. Then the TiO_2-P(MMA-AA-BA) (TP) nanospheres were obtained successfully.

2.3. Preparation of the composite separator

The 3D porous composite membranes were fabricated through non-solvent induced phase inversion process. The complete graphic illustration for the preparation process of composite membrane can be seen in **Scheme 1**. First, the PMIA solution was prepared by dissolving PMIA and LiCl in DMAc. Then, a certain amount of TP aqueous solution (2 wt %) was added into DMAc. Next, the mixture was stirred at room temperature to form a homogenous solution. The mixed solution was dropped slowly into PMIA solution (the mass ratio of mixed solution and PMIA solution was 1:1) with stirring for 12h, followed by sonicating for 0.5 h to obtain a homogenous casting solution (8 wt %). The obtained casting solution was uniformly coated on both sides of PE membrane by using doctor blade and then transferred to deionized water bath for 10 min at ambient temperature Then the TP-PMIA coatings were formed on both sides of PE membrane. Finally, the as-prepared TP-PMIA@PE composite membrane was further dried in a vacuum oven at 60 °C for 24 h. For comparison, the pristine PMIA-modified PE (PMIA@PE) membrane was prepared by the same procedure without adding of TP nanospheres. Meanwhile, a commercial PE separator was also investigated as a contrasting test in this study.

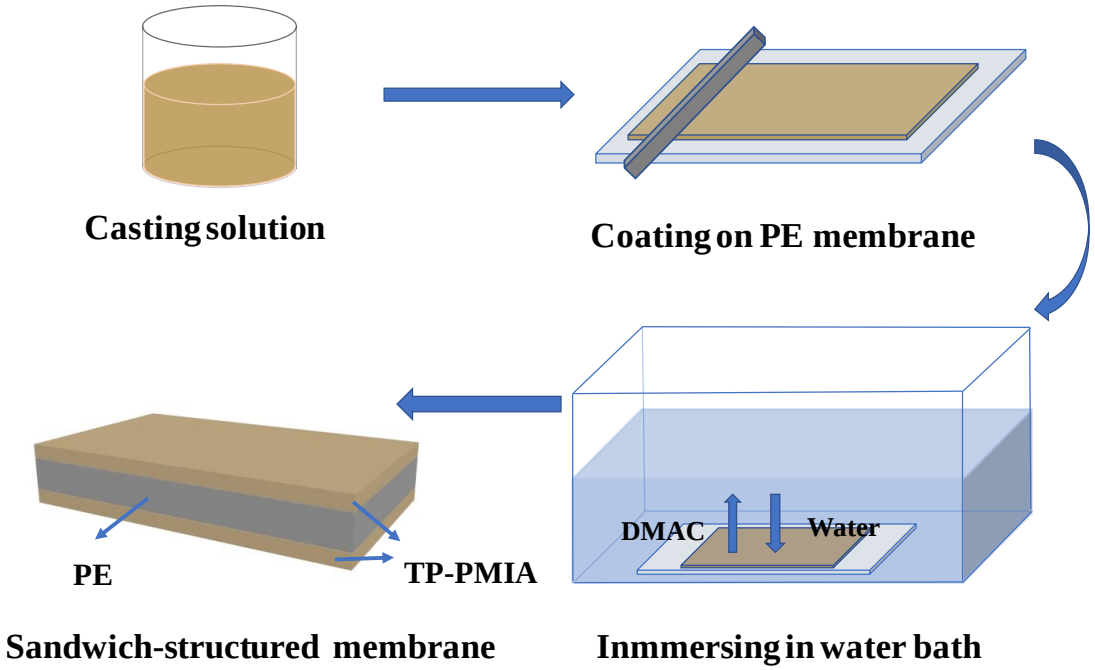

Scheme 1. The main fabrication procedure of the composite membrane.

2.4. Separator Characterization

The surface morphologies of the membranes were investigated by a field emission scanning electron microscope (FE-SEM, HITACH SU8010) at an acceleration voltage of 5 kV after sputtering with platinum. The micro-structure of the TP nanospheres was observed by a high-resolution transmission electron microscope (HR-TEM, FEI TECNAIG2 F30). The thermal property of membranes was studied by thermogravimetric analysis (TGA) at 10 °C min^{-1} from 50 to 800 °C under N_2 gas flow.

The thermal shrinkage of the membranes (size:3 cm×3 cm) was investigated by measuring the dimensional change after storing them in an oven at different temperatures (100 °C, 110 °C, 120 °C, 130 °C, 140 °C, 150 °C and 160 °C) for 0.5 h. The thermal shrinkage percentage (area-based) was calculated by the following equation.

$$Shrinkage\ (\%) = (S_0 - S_1)/S_0 \times 100\% \quad (1)$$

where the S_0 and S_1 represent the area of separators before and after the heat treatment, respectively.

Liquid electrolyte uptake measurement of the membranes was performed by immersing membranes in the electrolyte (1 M $LiPF_6$ in EC/DMC/EMC (1:1:1)) at 25 °C for 2 h in a glove box and then measured the weight change between the dry state and the soaked state of the membranes. The electrolyte uptake (U) was calculated according to the following equation.

$$U\ (\%) = (W_1 - W_0) \times 100\% \quad (2)$$

where the W_1 and W_0 refer to the mass of the soaked and dry membrane, respectively.

To study the wettability of the membrane, the electrolyte contact angle measurement of the samples was carried out by a contact angle goniometer (DSA30) in air atmosphere, where a droplet of electrolyte was dropped onto the surface of the membrane.

For the porosity testing, the membrane was immersed into n-butanol for 2 h until the equilibrium was achieved, and then the weight of the saturated and dry membranes was measured, respectively. The porosity was calculated by the following equation:

$$P\ (\%) = (M_1 - M_0)/(\rho \times V) \times 100\% \quad (3)$$

where P represents porosity of the membrane, M_1 and M_0 are the weight of the soaked and dry membrane, respectively, ρ is the density of the n-butanol, and V stands for the volume of the membrane.

2.5. Electrochemical performance

Ionic conductivity (σ) can be calculated according to the following formula:

$$\sigma = d/(R_b \times S) \quad (4)$$

where R_b is the bulk impedance (ohm), d indicates the thickness (cm) of the membrane, S represents the effective contact area between stainless steel discs and membrane. R_b was obtained by electrochemical impedance spectroscopy (EIS) using an electrochemical working station (Bio Logic Science Instruments) at room temperature.

The liquid electrolyte soaked membrane was sandwiched between the two stainless steel discs. The EIS tests were conducted at scanning frequencies ranging from 0.1 Hz to 100 kHz, with an amplitude of 5 mV.

The electrochemical stability window of the prepared membrane was investigated by linear sweep voltammetry (LSV) test. Before the measurement, the coin cell (lithium/separator/stainless steel) was assembled and sealed in the argon-filled glovebox. In our test, the stainless steel was used as the working electrode, while the lithium electrode as the reference and counter electrode, and the potential range was from 2.5 to 5.5V (vs. Li^+/Li) at 1 mV s^{-1}.

A LAND battery testing equipment (Wuhan, China) was used to evaluate the charge and discharge properties of the assembled button cell at room temperature. The coin-type half cell was assembled in a glove box filled with argon gas with the moisture and oxygen content below 0.01 ppm. The prepared membrane was used as separator, 1 M $LiPF_6$ in EC/DMC/EMC (1:1:1 vol), lithium metal and $LiFePO_4$ were employed as electrolyte, anode and cathode respectively. The $LiFePO_4$ cathode was prepared by mixing $LiFePO_4$ powder (80 wt%), Super P (10 wt%) and PVDF binder (10 wt%) in the N-methyl-2-pyrrolidone (NMP) solvent, then casting the slurry on the aluminum foil and drying at 60°C for 24 h. The charge/discharge cycling test was performed at a constant current density of 0.5 C for 100 cycles in a voltage window of 2.5 to 4 V at room temperature. For the rate performance measurement, the battery was charged and discharged at varied current densities of 0.2 C, 0.5 C, 1 C, 2 C and 5 C for 5 cycles respectively and finally returned to 0.2 C. Both cycle performance and rate performance measurements of the battery were activated at 0.1C for 3 cycles to form a stable solid electrolyte interface (SEI).

3. RESULTS AND DISCUSSION

3.1 morphology analysis

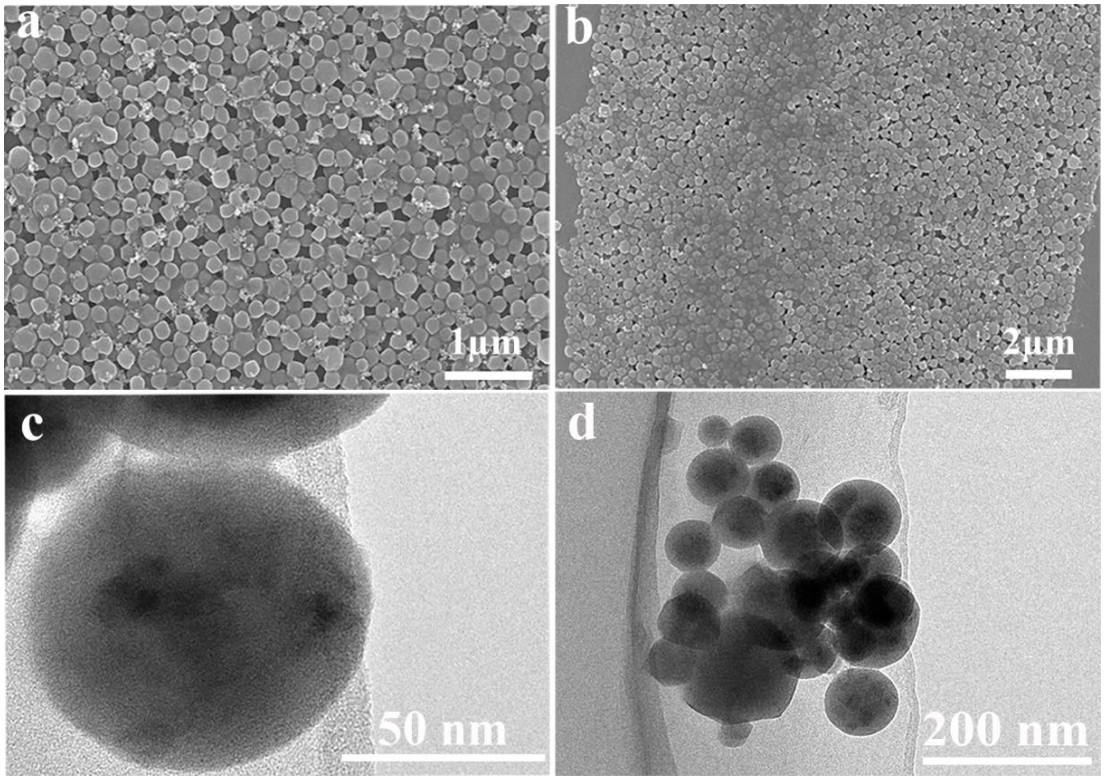

Figure 1. SEM images (a, b) and TEM micrographs (c, d) of the TP nanospheres

The core-shell structured TP nanospheres were synthesized. **Fig. 1** shows the SEM images (a, b) and TEM micrographs (c, d) of the as-prepared TP nanospheres. As can be seen from **Fig. 1a and b**,

these nanospheres exhibit a good monodisperse distribution and have a uniform spherical structure with an average diameter of 100 nm. The size and the core-shell structure of the TP nanospheres are obtained from the **Fig. 1c and d**, which are consistent with the SEM images. Such core-shell structure is similar to the structure of SiO_2-PMMA sub-microspheres reported by Yang [26] Every TP nanosphere is composed of the P(MMA-AA-BA) shell (light area) and several TiO_2 core particles (dark area) surrounded by P(MMA-AA-BA). TEM micrographs indicate that the TiO_2 particles are well encapsulated by P(MMA-AA-BA).

The pore structure of the separator plays an important role in the transportation of lithium ions, which further affects the electrochemical performance of the separator. The morphologies of the different membranes and the elemental mapping of TP-PMIA@PE composite membrane are shown in **Fig. 2**. It can be seen from **Fig. 2a** that the commercial PE separator possesses a large number of nanometer-size porous structure on the surface, which can prevent the penetration of electrode component particles and guarantee the migration of lithium ions. Compared with the PE membrane, the PMIA@PE membrane (**Fig. 2b**) and the TP-PMIA@PE composite membrane (**Fig. 2c**) show a homogeneous and smooth surface with similar pore size.

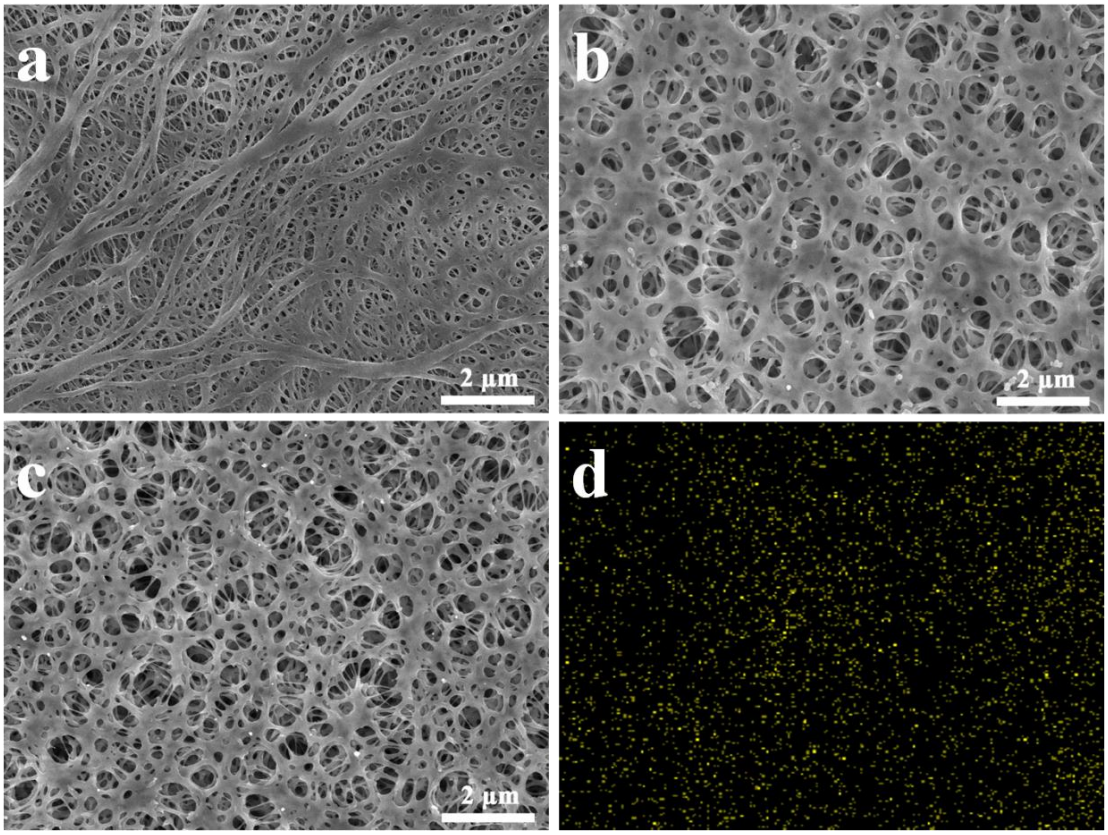

Figure 2. Surface SEM images of (a) the bare PE membrane, (b) the PMIA@PE membrane, (c) the TP-PMIA@PE composite membrane, (d) the element mapping images of Ti of TP-PMIA@PE composite membrane

Moreover, a highly interconnected network-like porous structure of blend membranes can be observed, which is formed during the mutual diffusion process between the solvent and non-solvent

[27,28]. It is consistent with the previous report [25] that the membrane exhibited numerous interconnected pores, which was beneficial for the storage of liquid electrolyte and migration of lithium ions [29]. This special structure is helpful to avoid blocking the pore structure of matrix. A uniform distribution of element Ti in the TP-PMIA@PE composite membrane is observed in **Fig. 2d**, suggesting that the TiO_2 nanoparticals in the membrane are distributed uniformly.

3.2 separator properties analysis

Various physical and chemical properties of the PE, PMIA@PE and TP-PMIA@PE membranes are summarized in **Table 1**. The thicknesses of the two kinds of composite membranes are 20 μm and 24 μm respectively, thicker than pristine PE membrane (12 μm). However, the thickness of the composite membrane is suitable for separator of LIBs in portable electronic devices and electric vehicle applications [30]. The porosity of a separator is a crucial factor for electrochemical properties of LIBs. As shown in **Table 1**, the porosities of the PMIA@PE (58%) and TP-PMIA@PE membranes (67%) are higher than pristine PE membrane (40%), owing to the interconnected porous structure formed by non-solvent induced phase inversion process [31]. The addition of TP nanospheres affects the formation of pore structure to some extent. The TP-PMIA@PE composite membrane with high porosity possibly exhibits high liquid electrolyte uptake, further leading to a high ionic conductivity, which is consistent with the paper in Cao [32].

Table 1. Physical and chemical properties of different membranes

Sample	Thickness (μm)	Porosity (%)	Electrolyte uptake (%)	Electrolyte contact angle (deg)	Ion conductivity (S cm^{-1})
PE	12	40	105	36	6.42×10^{-4}
PMIA@PE	20	58	202	10	6.00×10^{-4}
TP-PMIA@PE	24	67	254	8	7.90×10^{-4}

It is acknowledged that thermal stability of the separator is another vital parameter to evaluate the safety of batteries. A separator with good thermal stability can prevent internal short circuit of batteries at elevated temperature [33]. **Fig. 3a and b** show the photographs of PE, PMIA@PE and TP-PMIA@PE membranes before and after treating at 150 °C for 0.5 h, respectively. The PE membrane shows a serious dimensional shrinkage with obvious color change from white to transparent due to its inherent low melting point (130 °C) [30]. In contrast, the composite membranes of PMIA@PE and TP-PMIA@PE maintain the original dimension due to the introduction of high heat-resistance TP-PMIA coatings onto the both sides of the PE membrane [34,35]. The above results indicate that the composite membranes of PMIA@PE and TP-PMIA@PE can suppress thermal shrinkage effectively, further to prevent internal short circuit of batteries.

The dimensional shrinkage percentages (area-based) of PE, PMIA@PE and TP-PMIA@PE membranes at various temperatures for half an hour are shown in **Fig. 3c**. The commercial PE membrane exhibits a visible thermal shrinkage of 11% at 110 °C for 0.5 h and shows a remarkable dimensional shrinkage close to 100% when treated at 130 °C. In contrast, for PMIA@PE and TP-PMIA@PE membrane, there are almost no dimensional change until 150 °C and only have a shrinkage of 6% and 9% of the original area even at 160 °C, respectively. The dimensional shrinkage percentage of the TP-PMIA@PE membrane is a little higher than that of PMIA@PE membrane, which can be attributed to the higher porosity of TP-PMIA@PE membrane (**Fig. 2b and c**). The improvement of thermal stability by introducing coatings onto the membrane surfaces has been studied by many researchers. For example, Xi et al. prepared a composite membrane by coating PE membrane with TiO_2-PMMA nanoparticles. The thermal shrinkage is 29.6% at 140 °C for 0.5 h [36]. Ryou et al. fabricated the polydopamine-treated PE membrane that dimensional shrinkage is only 16% after treated at 140 °C for 1 h [17]. Remarkably, the PMIA@PE and TP-PMIA@PE membrane possesses good thermal stability compared with the aforementioned modified separators. The PE layer in the composite membranes can be also served as thermal shutdown layer, which is beneficial for enhancing the battery safety [37].

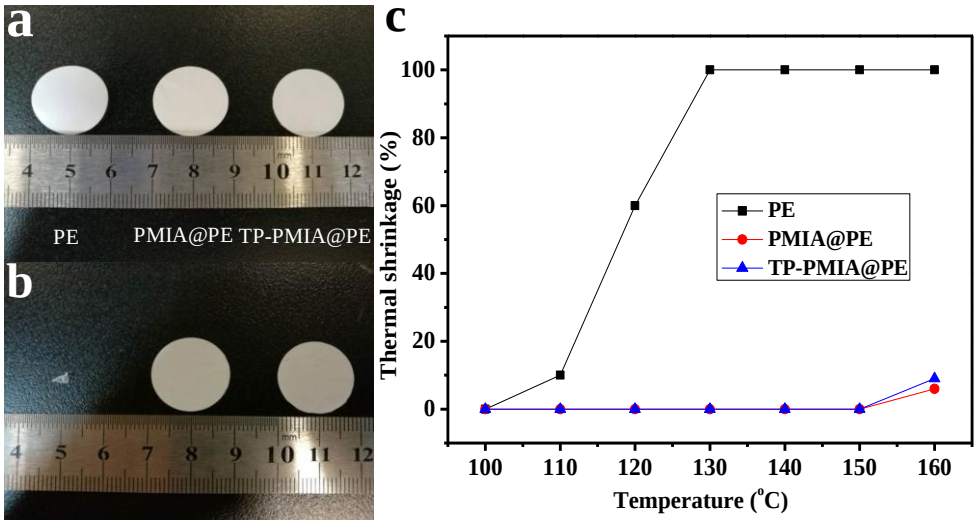

Figure 3. Photographs of the different membranes before (a) and after (b) treated at 150 °C for 0.5 h. (c) The dimensional shrinkage percent of different membranes at different temperature.

The thermal properties of TP-PMIA@PE membrane, PMIA-PE membrane and PE separator were further evaluated by thermogravimetric analysis (TGA) at 10 °C min^{-1} from 50 to 800 °C under N_2 gas (**Fig. 4**). For TP-PMIA@PE membrane and PMIA@PE membrane, a sharply weight loss can be observed at about 460 °C owing to the decomposition of the polyethylene backbone, and the remains (about 20%) are the coating layers on the composite membranes, which is confirmed by Wan [37].

The electrolyte wettability of the separator is also important for battery performance because good wettability can not only improve electrolyte uptake of the separator but also facilitate the migration of lithium ions between cathode and anode [38]. The wettability of the TP-PMIA@PE membrane,

PMIA@PE membrane and bare PE membrane is evaluated by the contact angle test, respectively. As shown in **Fig. 5a**, a certain amount of liquid organic electrolyte was simultaneously dropped onto the surface of each membrane and then the diffuse phenomenon of the electrolyte was observed.

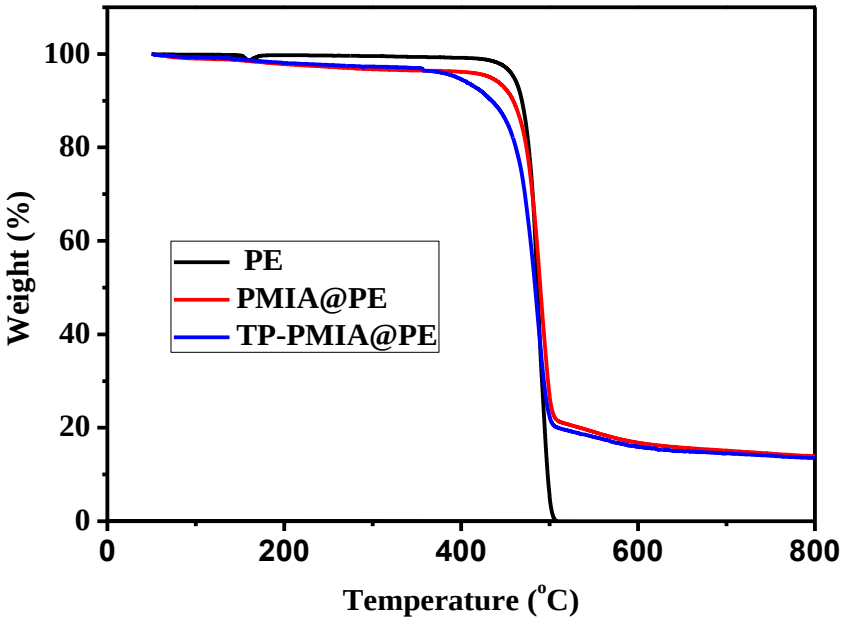

Figure 4. TGA curves of the bare PE membrane, the PMIA@PE membrane, the TP-PMIA@PE composite membrane.

The electrolyte droplet on the TP-PMIA@PE and PMIA@PE membranes spread quickly and became transparent due to the absorption of liquid electrolyte, whereas the electrolyte droplet was kept for a long time on the bare PE separator. **Fig. 5b** depicts that the electrolyte contact angles of the PMIA@PE and TP-PMIA@PE composite membranes are 10° and 8° respectively, which are much lower than that of the pristine PE membrane (36°), indicating a strong affinity towards liquid electrolyte of the composite membranes. The superior electrolyte wettability of the composite membranes can be ascribed to the presence of polar carbonyl groups and amine groups in PMIA and the TiO_2 nanospheres [25,34]. The inherent hydrophobicity of PE membrane results in poor wettability with liquid electrolyte.

The electrolyte uptake of the separator was measured by immersing membranes in the electrolyte in a glove box, summarized in **Table 1**. The high electrolyte uptake will facilitate the migration of lithium ions and is beneficial to improve the ionic conductivity, leading to superior rate capability of batteries. The TP-PMIA@PE and PMIA@PE membrane exhibit a high electrolyte uptake of 254% and 202%, respectively, which are much higher than that of PE membrane (105%). Therefore, the composite membranes possess the high electrolyte uptake, which is attributed to their excellent wettability with electrolyte and high porosity [39]. Moreover, the electrolyte uptake of the TP-PMIA@PE membrane is higher than that of PMIA@PE membrane due to the high porosity and the P(MMA-AA-BA) shells of TP nanospheres. The special structure of shells becomes gelled in the electrolyte after adsorbing a certain amount of electrolyte in the coating layers. [40].

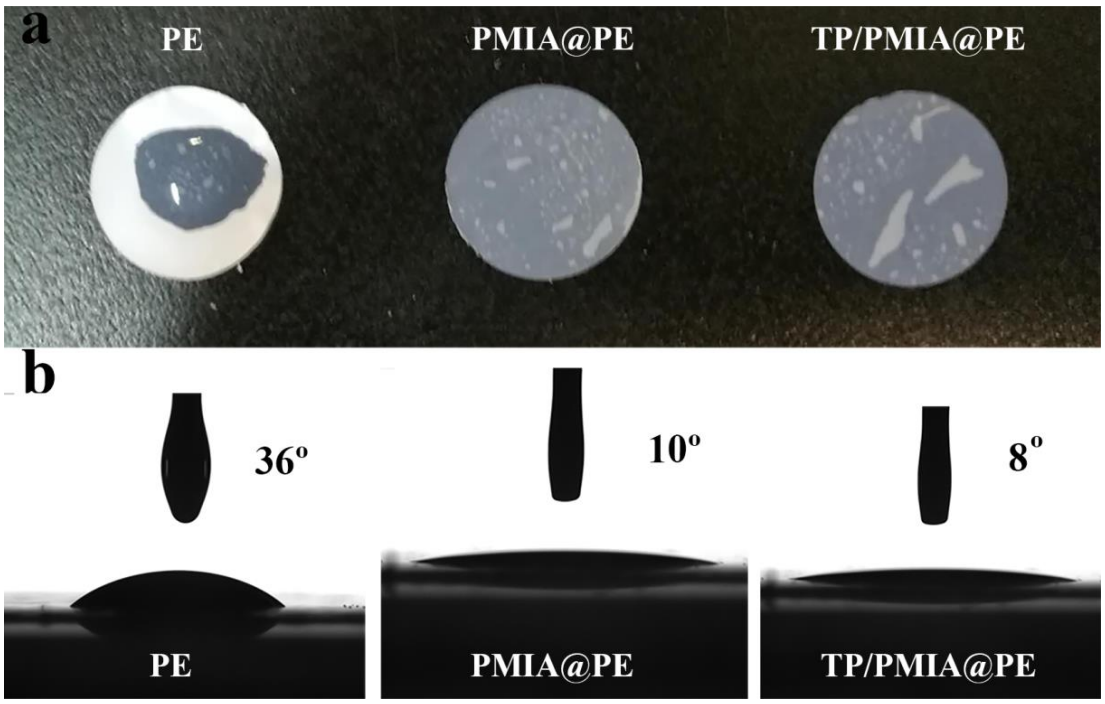

Figure 5. (a) Photograph of the wettability of PE membrane, PMIA@PE membrane and TP-PMIA@PE membrane with liquid electrolyte. (b) Electrolyte contact angles of different membranes.

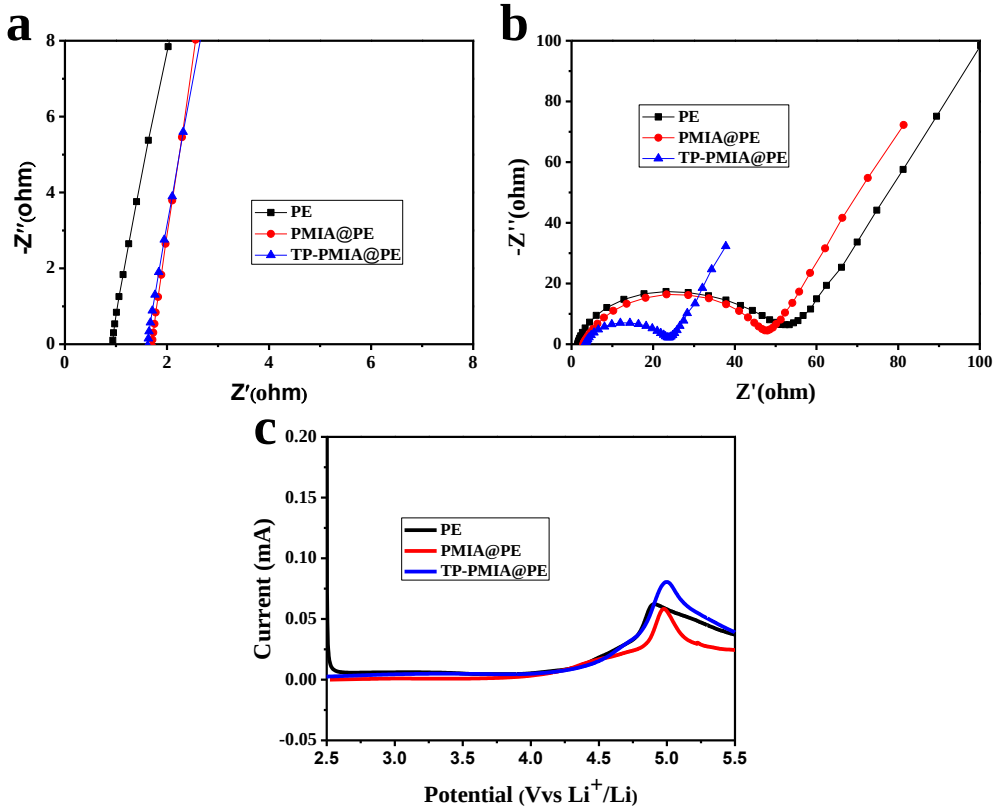

Figure 6. Electrochemical measurements of PE, PMIA@PE and TP-PMIA@PE membranes. (a) Nyquist plots with the different membranes, (b) AC impedance spectra of $LiFePO_4$/Li cells after 100^{th} cycle, and (c) Linear sweep voltammograms of Li/separator/SS cells.

The ionic conductivity of the membrane was studied by EIS tests at room temperature. The bulk resistance (R_b) was obtained from the Z' axis intercept in the Nyquist plot shown in **Fig. 6a**. Although the R_b of the pristine PE separator is a little lower than the PMIA@PE and TP-PMIA@PE composite membranes, the calculated ionic conductivity (0.79 mS cm^{-1}) of the TP-PMIA@PE (shown in **Table 1)** is higher than that (0.64 mS cm^{-1}) of PE membrane due to the higher thickness of TP-PMIA@PE membrane. By comparison, Li et al. developed a PBI/PE/PBI composite membrane with the ionic conductivity of 0.6 mS cm^{-1} [37]. And the ionic conductivity of TiO_2-grafted PE separator proposed by Zhu was 0.5 mS cm^{-1} [13]. Therefore, the TP-PMIA@PE membrane exhibits the high ionic conductivity, which should be ascribed to its high porosity with interconnected porous structure and the high electrolyte uptake due to the introduction of the PMIA and nano-TiO_2 hybrid [41]. The enhanced ionic conductivity of the TP-PMIA@PE membrane can facilitate the migration of lithium ions and further improve the rate capability of battery.

From **Fig. 6b**, it can be seen that AC impedance spectra of Li/$LiFePO_4$ cells with the bare PE, PMIA@PE and TP-PMIA@PE membranes after the 100th cycle at 0.5 C, are used to analyze the battery impedance. The left crossover point of the semicircle with the Z' axis represents the bulk resistance (R_b), which includes the resistance of electrodes, electrolyte and separator. The semicircle and straight line refer to the charge transfer resistance (R_{ct}) between the electrode and electrolyte and the Warburg impedance (Z_w) about the lithium ion diffusion in $LiFePO_4$ cathode, respectively [42]. The R_b of the PMIA@PE and TP-PMIA@PE membrane are slightly larger than that of the PE membrane because of the high thickness of the composite membrane. In contrast, the R_{ct} of TP-PMIA@PE membrane is far smaller than that of the bare PE and PMIA@PE membrane. The lower charge transfer resistance of TP-PMIA@PE membrane is mainly attributed to its excellent liquid electrolyte wettability and high porosity, facilitating the lithium ions migration and further improving the battery performance [43,44].

Electrochemical stability of the as-prepared membranes is a vital parameter for the application of battery, which was evaluated by linear-sweep voltammetry (LSV) tests [45], as shown in **Fig. 6c**. It can be observed clearly that the commercial PE membrane, PMIA@PE and TP-PMIA@PE composite membranes are all stable with no obvious anodic currents until around 4.5 V vs Li^+/Li. However, there is a considerable rise in current flow when the potential exceeded 4.5 V, which should be related to the oxidative decomposition of the membranes. Some reported research showed similar results [32,33,34]. The above result indicates that the composite membranes possess good electrochemical stability and can be applied to practical LIBs [34]. The rate capability of Li/$LiFePO_4$ batteries with different membranes was measured and shown in **Fig. 7**. The discharge capacities of all batteries with the different membranes gradually decrease with the increase of current density (**Fig. 7a-c**), ranging from 0.2 C to 5 C and finally returning to 0.2 C every 5 cycles. At relatively low discharge rates of 0.2 C, 0.5 C and 1 C, the discharge capacities are all very close for the three kinds of batteries (**Fig. 7d**). However, the difference in the discharge capacities increases obviously at high current densities of 2 C and 5 C, especially at 5 C rate, the cell with TP-PMIA@PE membrane exhibits a higher discharge-specific capacities of 128 mA h g^{-1} than that of the cells with PMIA@PE (114 mAh g^{-1}) and pristine PE membrane (116 mAh g^{-1}). The discharge capacity retention of the battery with TP-PMIA@PE membrane at 5 C is about 82% of that at 0.2 C, which is much better than that of batteries with PMIA@PE (75%) and PE membrane (72%). The excellent rate performance of the Li/$LiFePO_4$ battery with TP-PMIA@PE membrane is mainly attributed

to its excellent interfacial compatibility and its high ionic conductivity, which are favorable for lithium ions transport.

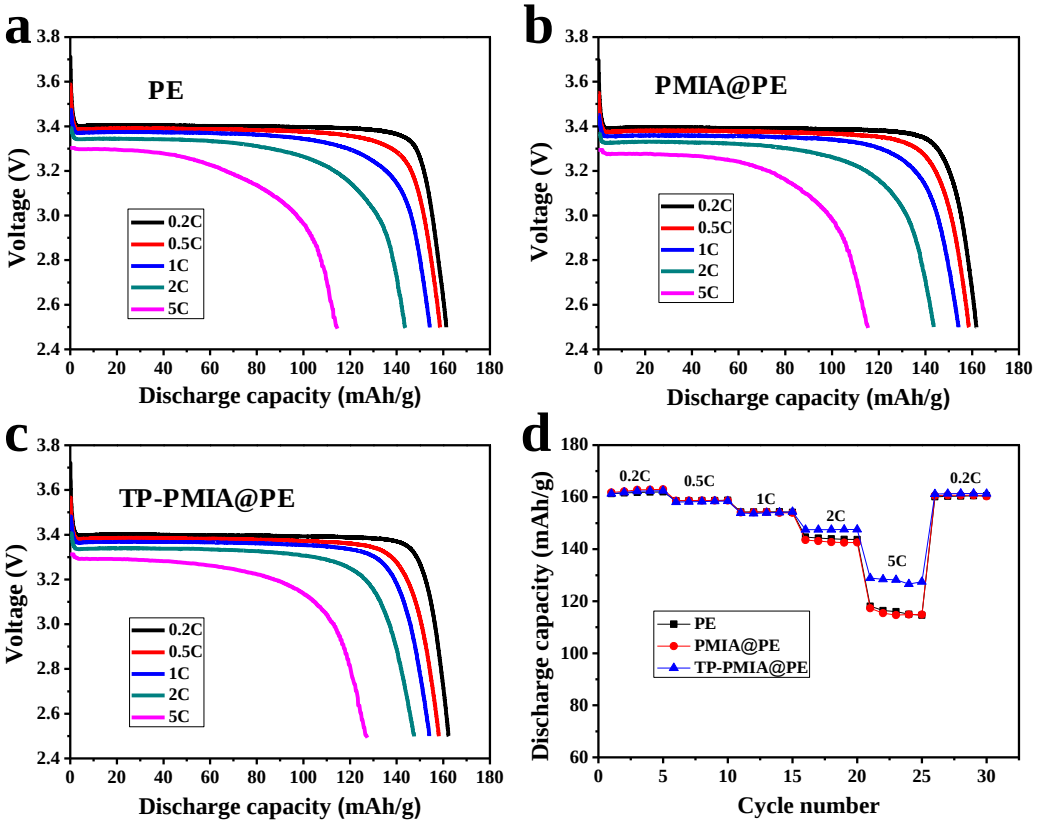

Figure 7. The discharge curves of $LiFePO_4$/separator/Li cells with (a) PE membrane, (b) PMIA@PE membrane and (c) TP-PMIA@PE membrane. (d) Rate performance of $LiFePO_4$/separator/Li cells with different membranes at the current densities of 0.2 C, 0.5 C, 1 C, 2C and 5C.

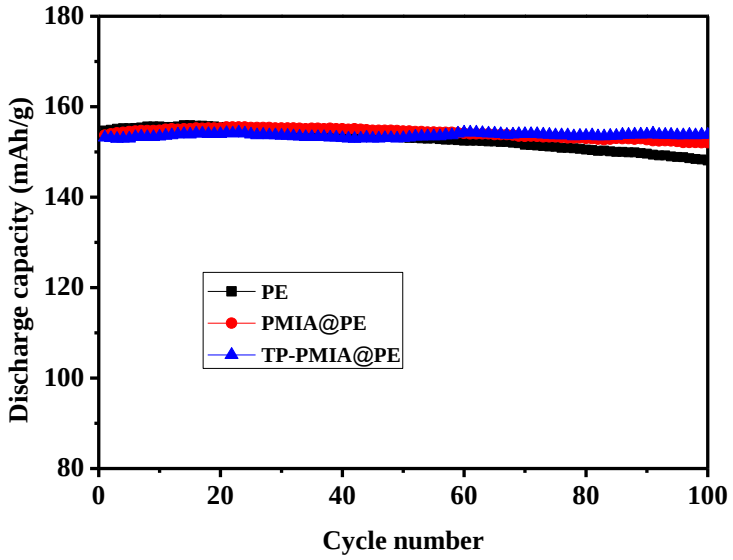

Figure 8. Cycling performance of the cells ($LiFePO_4$/separator/Li) with PE membrane, PMIA@PE membrane and TP-PMIA@PE membrane at 0.5 C.

Fig. 8 compares the cycling stability of Li/$LiFePO_4$ coin cells assembled with three kinds of membranes at 0.5 C under 2.5-4.0 V. For the cell with the TP-PMIA@PE membrane, the discharge capacity retention is up to 100% after 100 cycles and almost maintain its initial capacity, which is higher than the capacity retention of both PMIA-PE membrane (98.6%) and PE membrane (93.5%). The high capacity retention and stable cycle performance of the TP-PMIA@PE membrane are attributed to its highly developed nanoporous structure and superior affinity between membrane and electrolyte, which are favorable for lithium ions transport and interface stability.

Various physical and electrochemical performances of different composite membrane separators are listed in Table 2. It can be observed that the thermal stability, electrolyte uptake, ionic conductivity and specific capacity of the cells with TP-PMIA@PE membrane in this work are excellent or comparable to that of the cells with PE modified membranes in previous studies.

Table 2. Comparison of the various performance of other modified PE membrane separators

Sample	Thickness (μm)	Electrolyte uptake (%)	Thermal shrinkage (%)	Ion conductivity (S cm^{-1})	Specific capacity (mAh g^{-1})	Ref.
PDA-coated PE	25	126	16 (140°C,1h)	4.10×10^{-4}	139 (0.1C, Li/$LiCoO_2$)	[17]
SiO_2-PMMA@PE	25	89.5	13 (130°C,0.5h)	10.8×10^{-4}	107 (0.1C, graphite/$LiFePO_4$)	[26]
TiO_2-PMMA/PE	20	202	30 (140℃,0.5h)	8.70×10^{-4}	~130 (0.5C, Li/$LiFePO_4$)	[36]
PBI/PE/PBI	28	225	0 (200℃, 1h)	5.96×10^{-4}	~148 (0.5C, Li/$LiFePO_4$)	[37]
TP-PMIA@PE	24	254	0 (150℃,0.5h)	7.90×10^{-4}	154 (0.5C, Li/$LiFePO_4$)	This work

4. CONCLUSION

In this work, we successfully prepared a sandwich-structured TP-PMIA@PE composite membrane by a facile nonsolvent-induced phase inversion process. Compared with PE membrane, the obtained composite membrane possesses the improved physical and chemical properties by introducing nanoporous TP-PMIA coating layers onto both sides of PE membrane. The TP-PMIA@PE composite membrane shows high porosity (67%), excellent wettability with liquid electrolyte, high electrolyte

uptake (254%), low interfacial resistance and high ionic conductivity (0.79 mS cm^{-1}). In addition, due to the introduction of high heat resistance TP-PMIA coating layers, the TP-PMIA@PE membrane exhibits no dimensional shrinkage even at 150 °C. The battery assembled with the TP-PMIA@PE membrane shows excellent rate property and cycle performance. In summary, the experimental results clearly indicate that the TP-PMIA@PE composite membrane may be a promising candidate as separator for high-safe and high-rate LIBs.

ACKNOWLEDGMENTS
This work was supported by National Nature Science Foundation of China (51872157), Postdoctoral Innovative Talents Project of China (BX20190232), China Postdoctoral Science Foundation (2017M620771), Shenzhen Technical Plan Project (No.JCYJ20170817161753629, KQJSCX20160226191136 and JCYJ20170412170911187), Guangdong Technical Plan Project (No. 2015TX01N011) and Local Innovative and Research Teams Project of Guangdong Pearl River Talents Program (2017BT01N111).

References

1. S. Abada, G. Marlair, A. Lecocq, M. Petit, V. Sauvant-Moynot, F. Huet, *J. Power Sources*, 306 (2016) 178-192.
2. J.B. Goodenough, K.-S. Park, *J. Am. Chem. Soc*., 135 (2013) 1167-1176.
3. L.G. Lu, X.B. Han, J.Q. Li, J.F. Hua, M. Ouyang, *J. Power Sources*, 226 (2013) 272-288.
4. C.M. Costa, M.M. Silva, S. Lanceros-Mendez, *RSC Adv*., 3 (2013) 11404-11417.
5. H. Lee, M. Yanilmaz, O. Toprakci, K. Fu, X.W. Zhang, *Energy Environ. Sci*., 7 (2014) 3857-3886.
6. J. Moon, J.Y. Jeong, J.I. Kim, S. Kim, J.H. Park, *J. Power Sources*, 416 (2019) 89-94.
7. W.X. Xu, Z.Y. Wang, L.Y. Shi, Y. Ma, S. Yuan, L.N. Sun, Y. Zhao, M.H. Zhang, J.F. Zhu, *ACS Appl. Mater. Interfaces,* 7 (2015) 20678-20686.
8. J.H. Dai, C. Shi, C. Li, X. Shen, L.Q. Peng, D.Z. Wu, D.H. Sun, P. Zhang, J.B. Zhao, *Energy Environ. Sci.*, 9 (2016) 3252-3261.
9. J. Cho, Y.-C. Jung, Y.S. Lee, D.-W. Kim, *J. Membr. Sci*., 535 (2017) 151-157.
10. G.H. Feng, Z.H. Li, L.W. Mi, J.Y. Zheng, X.M. Feng, W.H. Chen, *J. Power Sources*, 376 (2018) 177-183.
11. C. Shi, J.H. Dai, X. Shen, L.Q. Peng, C. Li, X. Wang, P. Zhang, J.B. Zhao, *J. Membr. Sci*., 517 (2016) 91-99.
12. H. Chen, Q. Lin, Q. Xu, Y. Yang, Z.P. Shao, Y. Wang*, J. Membr. Sci*., 458 (2014) 217-224.
13. X.M. Zhu, X.Y. Jiang, X.P. Ai, H.X. Yang, Y.L. Cao, *J. Membr. Sci*., 504 (2016) 97-103.
14. J.-K. Pi, G.-P. Wu, H.-C. Yang, C.G. Arges, Z.-K. Xu, 9 (2017) 21971-21978.
15. S.Y. Hu, S.D. Lin, Y.Y. Tu, J.W. Hu, Y. Wu, G.J. Liu, F. Li, F.M. Yu, T.T. Jiang, *J. Mater. Chem. A*., 4 (2016) 3513-3526.
16. D. Lia, D.Q. Shia, Z.Z. Yuan, K. Feng, H.M. Zhang, X.F. Li, *J. Membr. Sci*., 542 (2017) 1-7.
17. M.-H. Ryou, D.J. Lee, J.-N. Lee, Y. M. Lee, J.-K. Park, J.W. Choi, *Adv. Energy Mater*., 2 (2012) 645-650.
18. Y. Guan, W. Li, Y.L. Zhang, Z.Q. Shi, J. Tan, F. Wang, Y.H. Wang, *Compos. Sci. Technol*., 144 (2017) 193-201.
19. J. Lin, S.H. Bang, M.H. Malakooti, H.A. Sodano, *ACS Appl. Mater. Interfaces*, 9 (2017) 11167-11175.
20. J.J. Zhang, Q.S. Kong, Z.H. Liu, S.P. Pang, L.P. Yue, J.H. Yao, X.J. Wang, G.L. Cui, *Solid State Ionics,* 245 (2013) 49-55.
21. K.S. Jeon, R. Nirmala, R. Navamathavan, K.J. Kim, S.H. Chae, T.W. Kim, H.Y. Kim, S.J. Park,

Mater. Lett., 132 (2014) 384-388.
22. Y.Y. Zhai, N. Wang, X. Mao, Y. Si, J.Y. Yu, S.S. Al-Deyab, M. El-Newehy, B. Ding, *J. Mater. Chem. A*., 2 (2014) 14511-14518.
23. W.M. Kang, N.P. Deng, X.M. Ma, J.G. Ju, L. Li, X.H. Liu, B.W. Cheng, *Electrochim. Acta*, 216 (2016) 276-286.
24. Y.F. Li, X.M. Ma, N.P. Deng, W.M. Kang, H.H. Zhao, Z.J. Li, B.W. Cheng, *Fibers Polym*., 18 (2017) 212-220.
25. H. Zhang, Y. Zhang, T.G. Xu, A.E. John, Y. Li, W.S. Li, B.K. Zhu, *J. Power Sources*, 329 (2016) 8-16.
26. P.T. Yang, P. Zhang, C. Shi, L.X. Chen, J.H. Dai, J.B. Zhao, *J. Membr. Sci*., 474 (2015) 148-155.
27. H. Strathmann, K. Kock, *Desalination*, 21 (1977) 241-255.
28. J.F. Kim, J.H. Kim, Y.M. Lee, E. Drioli, *AIChE J.,* 62 (2016) 461-490.
29. X.Y. Luo, Y.H. Liao, Y.M. Zhu, M.S. Li, F.B. Chen, Q.M. Huang, W.S. Li, *J. Power Sources*, 348 (2017) 229-238.
30. P. Arora, Z. Zhang, Battery separators, *Chem. Rev.*, 104 (2004) 4419-4462.
31. J. Heo, Y. Choi, K.Y. Chung, J.H. Park, *J. Mater. Chem. A*., 4 (2016) 9496-9501.
32. J. Cao, L. Wang, X.M. He, M. Fang, J. Gao, J.J. Li, L.F. Deng, H. Chen, G.Y. Tian, J.L. Wang, S.S. Fan, *J. Mater. Chem. A*., 1 (2013) 5955-5961.
33. D. Li, D.Q. Shi, K. Feng, X.F. Li, H.M. Zhang, *J. Membr. Sci*., 530 (2017) 125-131.
34. X.M. Zhu, X.Y. Jiang, X.P. Ai, H.X. Yang, Y.L. Cao, *J. Membr. Sci*., 504 (2016) 97-103.
35. J. Lin, B. Ding, J. Yang, J. Yu, S. S. Al-Deyab, *Mater. Lett*., 69 (2012) 82-85.
36. Y.Y. Xi, P. Zhang, H.N. Zhang, Z.H. Wan, W.M. Tu, H.L. Tang, *Int. J. Electrochem. Sci*., 12 (2017) 5421-5430.
37. D. Li, D.Q. Shi, Z.Z. Yuan, K. Feng, H.M. Zhang, X.F. Li, *J. Membr. Sci*., 542 (2017) 1-7.
38. Y. Xie, H.L. Zou, H.F. Xiang, R. Xia, D.D. Liang, P.C. Shi, S. Dai, H.H. Wang, *J. Membr. Sci.*, 503 (2016) 25-30.
39. Y.F. Chen, Y. Gao, J.J. Jian, Y.H. Lu, B.Y. Zhang, H.Q. Liu, L. Li, X.W. Wang, C.X. Kuang, Y.Y. Zhai, *Electrochim. Acta*, 292 (2018) 357-363.
40. M. Rao, J. Liu, W. Li, Y. Liang, D. Zhou, *J. Membr. Sci*., 322 (2008) 314-319.
41. W.-K. Shin, D.-W. Kim, *J. Power Sources*, 226 (2013) 54-60.
42. R. Ruffo, S.S. Hong, C.K. Chan, R.A. Huggins, Y. Cui, *J. Phys. Chem. C*, 113 (2009) 11390-11398.
43. J. Shi, Y. Xia, S. Han, L. Fang, M. Pan, X. Xu, Z. Liu, *J. Power Sources,* 273 (2015) 389-395.
44. Z. Li, W.Q. Wang, Y. Han, L. Zhang, S.S. Li, B. Tang, S.M. Xu, Z.H. Xu, *J. Power Sources*, 378 (2018) 176-183.
45. N. H. Idrisa, M. M. Rahmana, J. Z. Wang, H. K. Liu, *J. Power Sources*, 201 (2012) 294-300.